Spring 2023

Wetting Transition of Texturized Surfaces

Jenna Stephens
The University of Akron, jps117@uakron.edu

Table of Contents

Executive Summary

In continuation of work completed by previous students, this project aimed to investigate the fabrication and surface energy modification of long-lasting, textured, 3D printed hydrophobic surfaces. These surfaces were designed using principles of biomimicry by investigating naturally occurring textured surfaces that show hydrophobic and hydrophilic properties, such as desert beetle backs (hydrophilic) and cicada wings (hydrophobic). The 3D models were designed to be uniform arrays of cylindrical pillars of specified height, diameter and spacing, and were intended to excel at repelling water while effectively trapping oil compounds. Development of these technologies would be useful in a variety of applications such as oil recovery, water purification, self-cleaning surfaces, anti-fouling, anti-fogging, and corrosion prevention.

The primary goal of this segment of the project was to find appropriate 3D printing equipment and methods for fabricating new textured surfaces with improved quality and performance. To do this the Flashforge Foto 8.9 4K Mono LCD Resin 3D Printer with Anycubic 405 nm UV sensitive white resin, was selected. The new printer has improved printing accuracy of 50 μm compared to 200 μm for the previous printer. Along with adjustments to settings and cleaning procedures, the new printed models had 42-78% less deviation in the pillar heights and 38% less deviation in the width of the pillars. Also, the pillar heights of the new models were more accurate to the design parameters as they no longer had undesirable hemispherical dome shaped tops that resulted hysteresis due to increased contact area with liquids placed on the surface. When the performance of new models was compared with old models, of the same specified dimensions, by water drop contact angle experiments, the new models were comparable to the old models and showed some improvement, which indicated that the new models were an adequate, if not better, replacement for the old models.

The secondary goal of this project was to investigate the 3D models' surface properties both with and without additional surface modifiers for their ability to repel water and absorb octane (chosen to represent oil compounds). The first portion of these experiments were previously investigated by other students using the old models and were repeated in this project using the new models. New models of the same design specifications (1000μm height, 500μm diameter, 250μm edge to edge spacing) were either left untreated, treated with octadecyl trichlorosilane (OTS), or perfluoro organosilane (FTS). The untreated models effectively absorbed the octane and repelled the water individually, but when a mixture of water and octane were placed on the surface small amounts of water ended up being partially absorbed due to the movement of the octane in between the pillars. The OTS treated model effectively absorbed the octane and repelled the water completely. The FTS treated model repelled both the octane and water. These results aligned with what was expected based on the surface treatments. When experiments to measure the vertical liquid uptake into the model surfaces were performed, the related results were observed. The untreated model had uptake heights of 15.5 mm and 0.5 mm for octane and water, respectively. The OTS treated model had uptake heights of 10 mm and 0 mm for octane and water, respectively. The FTS treated model did not uptake octane nor water.

In conclusion, this project successfully identified and selected a new printing method for fabricating textured 3D models that improved the quality compared to old models. This is shown by improvements in the deviations of the heights and diameters of the pillars, and the comparable performance of the new models to the old models. This project also determined that both the untreated and OTS treated models can repel water and absorb octane, but the OTS treated models do it more effectively as they did not absorb any water while the untreated models absorbed a small amount of water. It is recommended that future work on this project includes the

completion of additional uptake experiments using models with increased pillar height as well as assessing the limits of the printer by creating models with smaller features (diameter and spacing) that more closely resemble naturally occurring hydrophobic surfaces such as cicada wings.

By working on this research project, I gained experience in project planning and execution, and learned more about how to adapt when plans do not always go as expected. These skills are extremely valuable, and I know they will help me be a more successful and effective chemical engineer. I also learned a lot about 3D printing, which I did not know much about previously. I believe that this experience encouraged me to apply both my technical knowledge and creative problem-solving skills. On a broader scale, this research project helped expanded upon previous research that could be beneficial to society in a variety of ways such as water and oil separation for oil spill cleanup and corrosion prevention.

Introduction

The use of biomimicry in the development of innovative technologies has been around for centuries. Inspiration from nature has been used in the design of watercrafts, airplanes, Velcro, and architecture[1]. For years we have looked to nature for inspiration on how to solve problems that evolution has already taken care of for other species. This project uses biomimicry concepts to look towards nature for ways to develop surfaces that selectively repel or attract different liquids. Specifically, to develop surfaces that repel water and absorb other fluids such as oils. These technologies would be useful in a variety of applications such as oil recovery, water purification, self-cleaning surfaces, anti-fouling, anti-fogging, and corrosion prevention.

Hydrophobic and hydrophilic surfaces have long held an evolutionary advantage for various plants and animals. Hydrophilic surfaces can be used to capture or store water for use later, this is the case for one of many fog-harvesting desert beetles *Stenocara gracilipes*[2]. The textured hydrophilic surface of *Stenocara gracilipes* is shown in **Figure 1**. This textured surface harvests water from fog and directs it towards the beetle's mouth where it can be consumed.

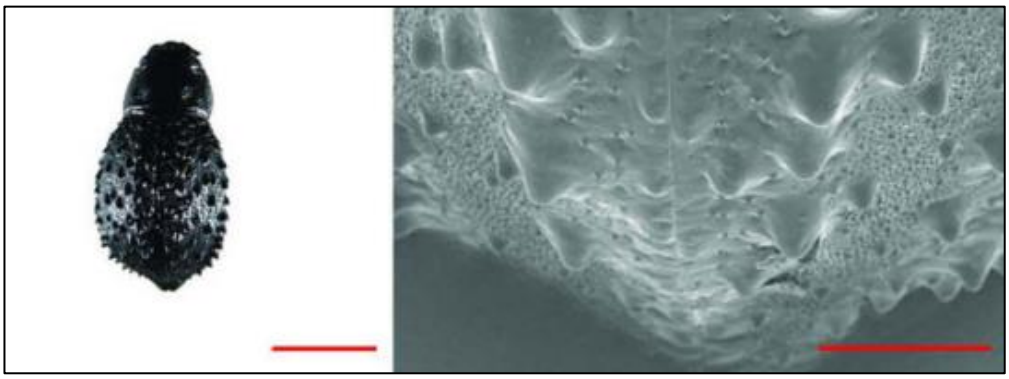

Figure 1: Left: extended depth focus image of the back of *Stenocara gracilipes* with a scale bar of 5mm[2]. Right: scanning electron microscope (SEM) image of the textured surface of the back of *Stenocara gracilipes* with a scale bar of 1 mm[2].

Hydrophobic surfaces are used to repel water for the purpose of self-cleaning, preventing rot or quickening dry times once wet, which is seen on *psaltoda claripennis,* cicada, wings[3]. The cicada wings feature microscopic pillars that repel water, shown in **Figure 2**. The homogenous pattern of pillars on the cicada's wings effectively remove water which is advantageous to its survival.

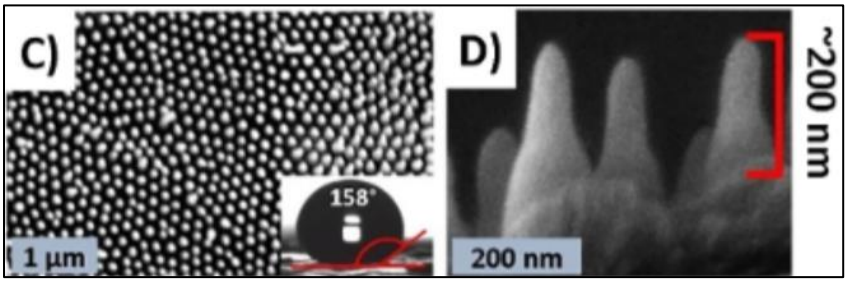

Figure 2: Left: top-down SEM view of a cicada wing to show the pillar array[3]. Center: contact angle of a water drop placed on a cicada wing[3]. Right: SEM side view of cicada wing texture to show pillar size and shape [3].

Previous work conducted on this topic by University of Akron students, Hannah Pineault, and Isabelle Moryan, set the groundwork and launched the investigation of the effectiveness of 3D printed surfaces modeled after hydrophobic surfaces seen in nature. In their studies, 3D models of pillar arrays were designed and fabricated using a resin-based 3D printer to have dimensions on the scale of hundreds of microns that mimic the pattern found on naturally hydrophobic surfaces. Then each surface was evaluated for water droplet and organic solvent droplet contact angles. Additionally, the surfaces were treated with a variety of surface energy modifiers to increase the hydrophobicity[4][5].

During the previous investigation one source of error was found to be the shape and uniformity of the 3D printed surfaces. Each of the pillars on a given model were designed to have uniform diameters, spacing and heights with flat tops, but unfortunately due to the use of filament and the printer's capabilities, the pillars ended up having hemispherical dome shaped tops, which would increase the area of contact[4][5], thus more interactions between the surface and the liquid, resulting in a greater contact angle hysteresis. An image of one of the previous 3D printed models is shown in **Figure 3** alongside the 3D drawing of the model to represent how the print should ideally look.

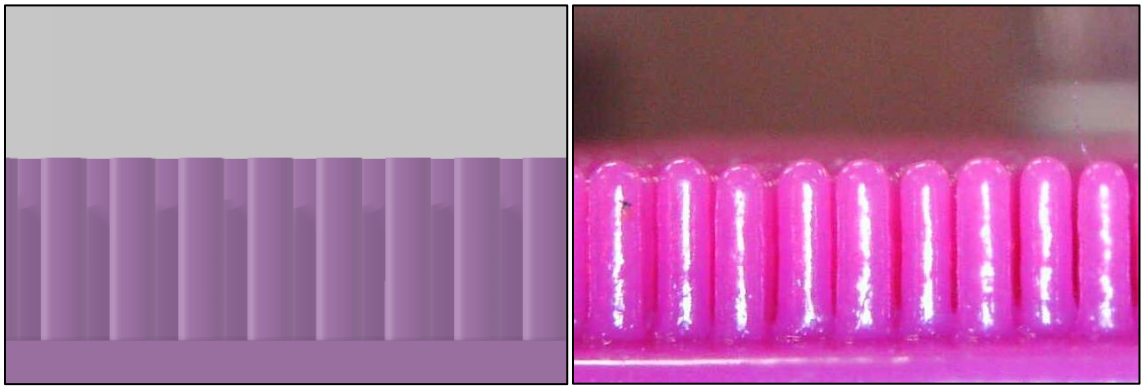

Figure 3: Left: the 3D drawing of the model. Right: one of several 3D printed surfaces fabricated by Hannah Pineault during the first phase of this project[4]. Each pillar has a diameter of 500 microns and height of 2mm.

The first objective of the new phase of this project is to determine if the 3D model uniformity issues could be reduced or eliminated by using a resin 3D printer with an improved resolution. To determine how successful the new models are, pillar size measurements (diameter and height) and water droplet contact angle measurements were taken and compared to those of the old models. Once the first objective was met, the secondary object was to investigate additional properties of the new 3D model surfaces both with and without the application of surface energy modifiers. This included the separation of water and octane droplets and the uptake of water and octane individually when the edge of the surface is submerged in liquid.

Background

The first goal of this project was to investigate how to improve the quality of the 3D printed models. The printer that was used previously was the Stratasys Objet260 Connex3 polyjet printer with curable photopolymer VeroCyan™ ink[4]. This resin-based printer has a layer resolution of 16 mm and an accuracy of 200 mm. The typical 3D models are designed to have pillars of 500 mm diameter, 1000 mm height and 750 mm spacing (center to center distance of pillars) in a hexagonal array. Since the previous models had issues with the consistency of pillar sizes (diameter and height) it was determined that improving the printer accuracy would be most beneficial even if the layer resolution were slightly less.

To do this the Flashforge Foto 8.9 4K Mono LCD Resin 3D Printer with Anycubic 405nm UV sensitive white resin was selected. This printer has a layer resolution of 25 μm and an accuracy of 50 μm and was determined to be one of the more affordable options with these specifications[6]. With increased accuracy, the printer would be able to produce more defined edges of the pillars and ultimately create a more uniform model that is true to the design parameters. Additionally, the improved parameters mean that, in future designs, the models' dimensions could be scaled down to investigate different properties more like those commonly found in nature.

Printing 3D models with resins printers requires more than just obtaining a printer and selecting a resin. Several steps in the printer preparation and post-printing cleaning had to be determined to ensure optimal print quality. In preparation for printing, the build plate needed to be clean and leveled, while the resin in the resin reservoir needed to be filtered to remove any fine particulates that may become trapped in the cured print. **Figure 4** indicates the various parts of the 3D printed mentioned previously. For post-printing cleaning, each of the semi-cured models must be thoroughly rinsed in isopropyl alcohol then blown dry with pressurized air to remove any trapped uncured resin from between the pillars.

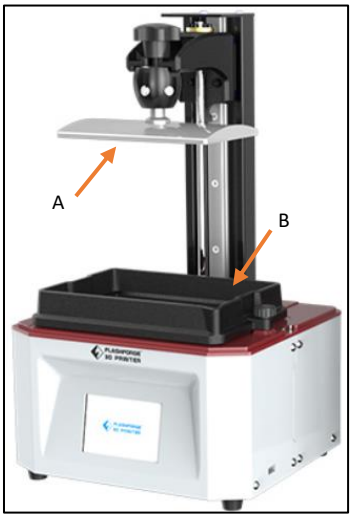

Figure 4: A picture of the Flashforge Foto 8.9 4K Mono LCD Resin 3D Printer[6]. The build plate (the surface which the model gets printed onto) and resin reservoir (the containment area for uncured resin and the location of active layer printing) are labeled A and B, respectively.

As for the secondary goals of the project, contact angle and liquid uptake experiments were conducted and the results analyzed. Contact angle is the quantitative measure of a liquid wetting a solid and is defined by the angle that the liquid creates between the liquid-solid interface and the line tangent to the three-phase contact line[7]. An illustration of a contact angle measurement is provided in **Figure 5**. The more hydrophobic a surface is, the greater the water contact angle will be. Therefore, this project aims to create surfaces that will result in large water contact angles.

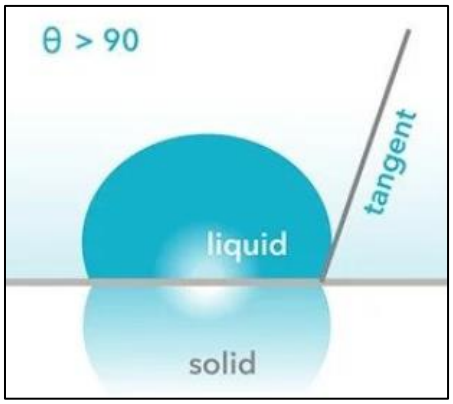

Figure 5: An illustration of how contact angle is measured [7].

The liquid contact angle on a textured surface depends on the surface's ability to trap air between the grooves and thus effectively repel the liquid. If the air remains trapped and the liquid does not penetrate the surface, the liquid is said to be in the Cassie-Baxter state. When the air gets displaced and the liquid penetrates the grooves, the liquid is said to be in the Wenzel state. The criterion for liquid penetrating the grooves is given by Equation 1. If the criteria are not satisfied, air trapping inside the grooves becomes possible and the Cassie-Baxter state can be obtained. In this equation q_s is the intrinsic contact angle between the liquid and the smooth surface of the material, f_s is the areal fraction of the material, and r is the surface roughness.

$$cos\theta_s \geq \frac{1-f_s}{r-f_s} \qquad \text{when } \theta_s < 90° \tag{1}$$

Once the criteria have been evaluated, the apparent contact angle (θ_{app}) for the predicted state can be calculated. This estimated angle can then be compared to experimental values to confirm whether the liquid droplet is closer to the Cassie-Baxter state or Wenzel state. The equation for $\theta_{app,\,Cassie\text{-}Baxter}$ is given in by Equation 2 and $\theta_{app,\,Wenzel}$ by Equation 3.

$$cos\theta_{app,Cassie-Baxter} = f_s cos\theta_s - (1 - f_s) \tag{2}$$

$$cos\theta_{app,Wenzel} = r cos\theta_s \tag{3}$$

For experimental droplet contact angle analysis, the liquid is assumed to be in the Cassie-Baxter state initially, based on the predicted apparent contact angle, and the observation that the interface of the liquid is in contact with both the solid surface of the pillars and the air that is trapped between the pillars. This initial contact angle and transition can be seen from a sideview of the surface when a droplet is placed upon it, however due to obstructed visibility from the rest of the surface pillars it is easier to take measurements of the droplet radius from above and relate it to the contact angle. This is demonstrated in **Figure 6**.

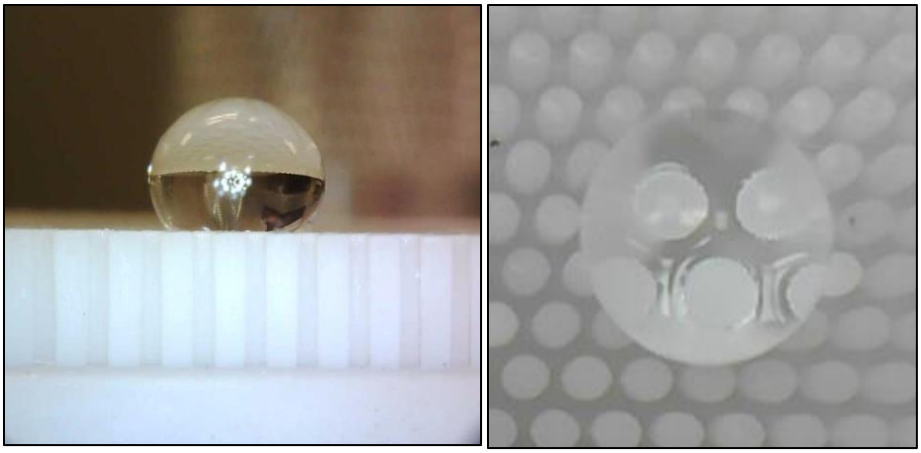

Figure 6: Left: the side view of a water droplet in the Cassie-Baxter state. Right: the top-down view of the same water droplet which can be used for contact angle measurements.

To determine the contact angle of the droplet from the top-down view, the radius (R) along with the drop volume (V) is input into equations that calculate the contact angle (q). Equation 4 is used for angles less than 90°, while equation 5 is used for angles greater than 90°. Since, for all contact angle experiments in this project, the droplet volume was known, and the radius was easily measured these equations simplified and increased confidence in contact angle measurements.

$$V = \frac{\pi}{3} R^3 (2 + cos\theta)(1 - cos\theta)^2 \qquad \text{where } q<90° \quad (4)$$

$$V = \frac{4\pi}{3} R^3 - \frac{\pi}{3} R^3 (2 - 3\cos(180 - \theta) + \cos(180 - \theta)^3) \qquad \text{where } q\geq 90° \quad (5)$$

Experimental Methods

Both the old models (ones printed using the Stratasys Objet260 Connex3 polyjet printer) and the new models (ones printed using the Flashforge Foto 8.9 4K Mono LCD Resin 3D Printer) used the same 3D sketch design, which specified the dimensions and array of the pillars. The cylindrical pillars were designed to be in a hexagonal array with diameter (D), height (H) and edge to edge pillar spacing (S). For this phase of the project, D was held constant at 500 mm, S was held constant at 250 mm, while H was either 1000 mm or 2000 mm.

When fabricating the new models, the following steps were taken to ensure the quality of the models. The 3D printer build plate was sanded to improve the adhesion of the semi-cured model to the plate and prevent unwanted bending or detachment during the printing process. When the semi-cured models were removed from the build plate, extra caution was used to ensure that they were not being bent or the pillars dislodged. Before the final UV curing step, each model was washed thoroughly using a rinse bottle filled with isopropyl alcohol, then dried using a stream of pressurized air supplied to the lab hoods. Finally, the models were UV curved for 30 minutes.

The surface modifiers that were used to treat the models were perfluoro organosilane (FTS) and octadecyl trichlorosilane (OTS). The process of depositing modifiers to the models' surfaces included the following procedure. First, the models were rinsed with DI water, acetone, and isopropyl alcohol, then dried with pressurized air intermittently to remove residues. Next, they were oxidized by air plasma treatment with a radio frequency power of 18 W for 10 minutes in a Harrick Plasma Cleaner PDC-32G. Then, the models were submerged in 0.5 wt.% FTS or OTS in hexane solution, depending on the desired treatment, for 1 hour. Finally, the models were removed, rinsed with hexane, dried, and left under a heat lamp for at least 30 minutes to ensure the modifiers were as adhered to the model's surface as possible.

For the water droplet contact angle experiments, 10 mL of DI water was dispensed using a precision pipet, to maintain consistency, onto the pillared surface of the model. Pictures of the droplet were taken from the top view at an interval of one second for 30 minutes. After the experiment, the pictures were analyzed using ImageJ to obtain five circumference measurements which were used to determine the radius of the droplet. The radius was then used, as previously described, in equations 5 and 6 to determine the contact angle. This procedure was used for all the surfaces regardless of treating with organosilanes.

For liquid uptake analysis, both water and octane were evaluated individually on 3D models that were either un-modified, oxidized, OTS treated, or FTS treated. The 3D model was mounted vertically such that the pillars were parallel to the liquid interface. A small glass container holding approximately 20-40 mL of liquid was placed on a balance which was connected to a computer to record mass measurements every one second. Also, a camera was aimed at the 3D model's surface to record any visual indications of liquid uptake. Analyses of results of liquid mass uptake and liquid travel up the model's surface (i.e., liquid height) using ImageJ of the images were conducted.

Data and Results

New 3D models were fabricated using the Flash Forge Foto 8.9 resin 3D printer and were designed based on the same feature dimensions as the old 3D models used by Hannah and Isabel. Qualitatively, the new prints were more uniform and resembled the software generated design more closely. In **Figure 7**, the new printed pillars (white, A & C) have well defined edges and are much more uniform compared to the old prints (pink, B & D). Additionally, the new prints have flat tops, as designed, and eliminate the dome shaped defect that was previously suspected to increase contact angle hysteresis.

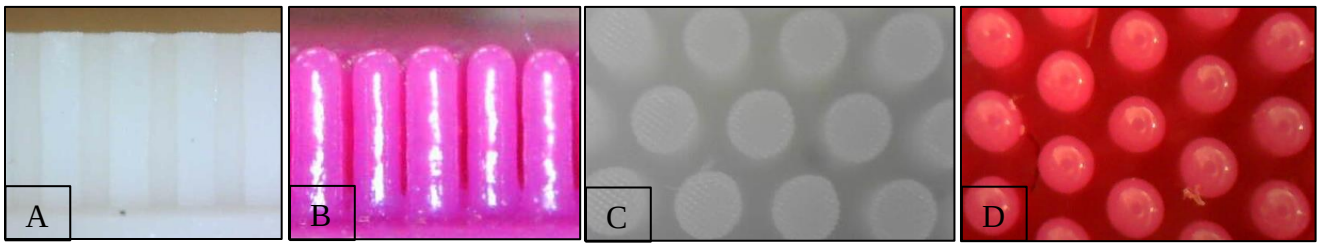

Figure 7: Side by side comparisons of the new (white, A and C) and old (pink, B and D) D0.5 H2 S0.25 3D models.

Measurements of the heights and diameters of 15 randomly selected pillars from each of the four 3D models were taken and used to quantify the improvements noted above. When comparing two models designed to have the same heights, the new prints consistently were closer to the intended height size and had lower standard deviations as shown in **Figure 8**. This was confirmed by t-test which proved that the heights of the new models are different from the old models. When comparing the diameters of the models it was found that the new models had smaller standard deviations, seen in **Figure 9**, thus were more uniform. However, based on t-test results the average diameter of a new model versus and old model could not be proven different. A summary of the statisitcal analysis can be found in **Appendix B.**

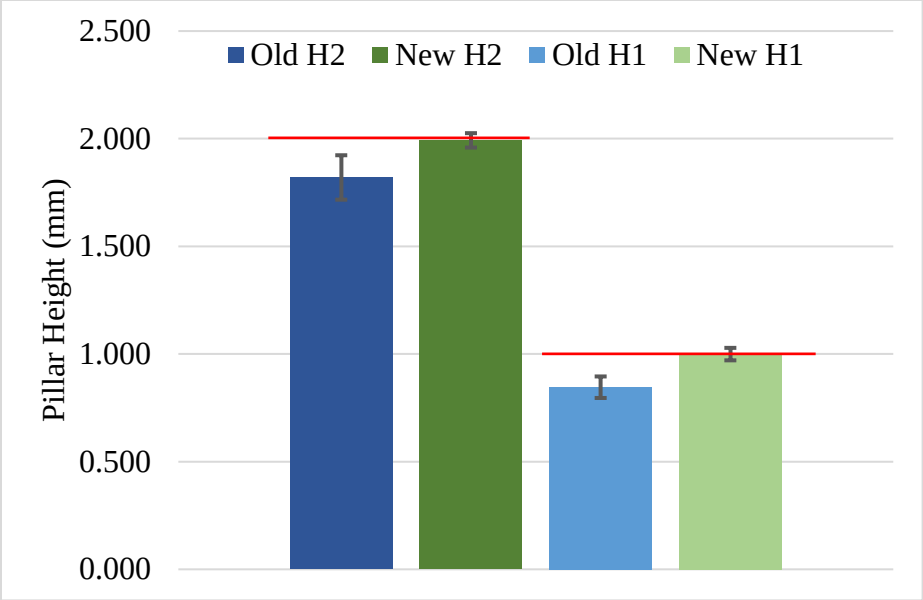

Figure 8: Height comparisons for the new and old 3D models with error bars representing the standard deviation. The red lines indicate the data sets that are compared for the given height that the models were designed to be (1 mm or 2 mm).

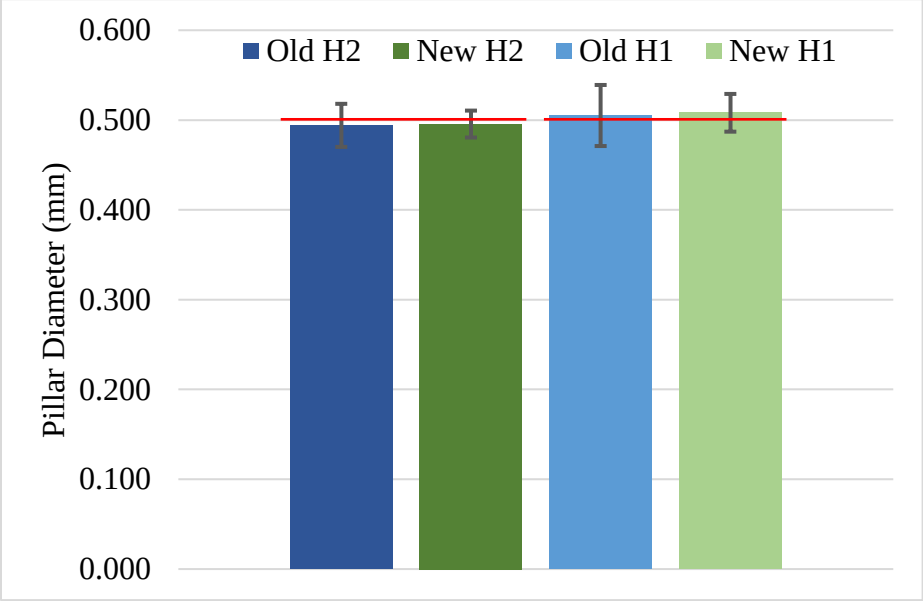

Figure 9: Diameter comparisons for the new and old 3D models with error bars representing the standard deviation. The red lines indicate the data sets that are compared for the given diameter that the models were designed to be (0.5 mm).

Next, to compare the performance of the new prints to the old prints, initial water droplet contact angles were measured. The prints all had diameters of 0.5 mm, edge to edge spacing of 0.25 mm, and heights of either 1 mm or 2 mm. This was done for new and old prints both untreated and treated with OTS. The average contact angles for each surface were measured five times and analyzed using the Minitab one-way ANOVA tool. It was found that only the untreated new models with a height of 1 mm and 2 mm were significantly different from the OTS treated old model with a height of 1 mm. However, those models were not able to be proven different from

other models tested. The results are summarized in **Figure 10** and the detailed one-way ANOVA results can be found in **Appendix C**.

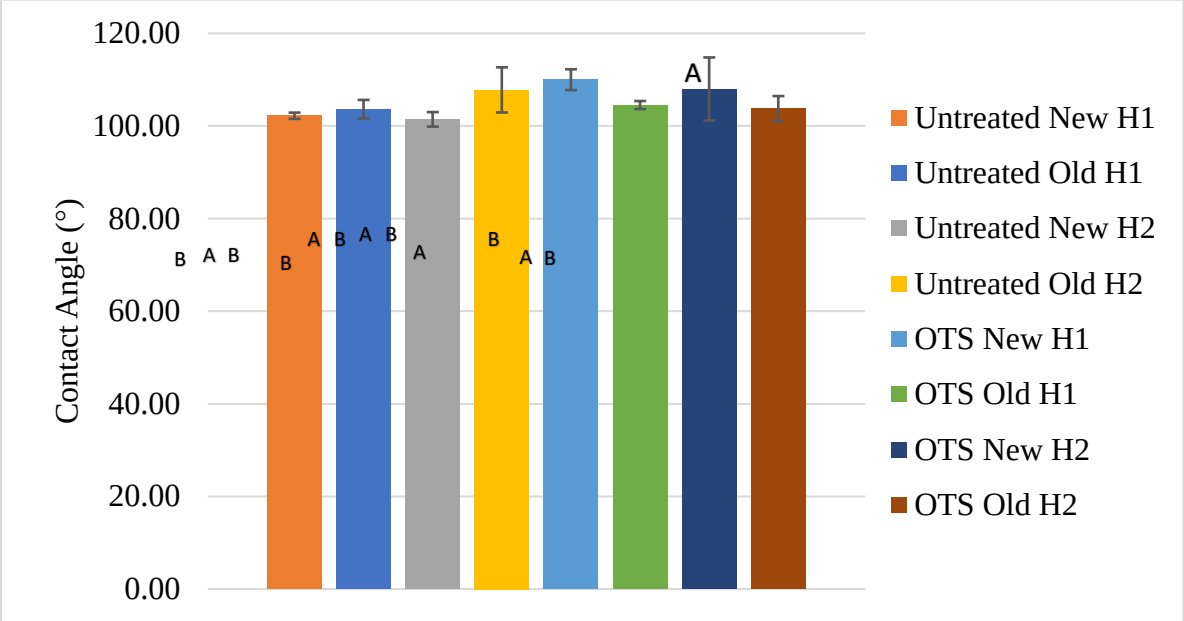

Figure 10: Average water drop contact angle with error bars representing standard deviation. The surfaces had three varied parameters of new or old print method, untreated or OTS treated, and height of 1 mm or 2 mm. The letter above each bar represents the results of the one-way ANOVA test where sets that do not share a letter are considered to have statistically different averages.

During the contact angle measurement experiments, contact angle hysteresis of the old models was identified and briefly investigated. When a water drop was placed on an old and new surface of the same dimensions and treatment and one edge was raised incrementally at an angle, the drop began to roll at approximately 46° on the new model, but never rolled off the old model. This is thought to be a result of the old models having hemispherical shaped tops to each pillar while the new models have flat tops. Images of this finding are shown in **Figure 11**.

Figure 11: Pictures of the behavior of 10mL water droplets on new and old 3D printed models with surface measurements of height = 2 mm, diameter = 0.5 mm and edge to edge spacing = 0 .25 mm.

Moving on to investigate the ability of the new models to absorb octane, three new models of the same dimensions were either left untreated, treated with OTS or treated with FTS. This

experiment was previously conducted by Isabel Moryan using the old models[5]. Consistent results were exhibited by the new models. The untreated and OTS treated samples both absorbed the octane instantaneously, while the FTS model did not absorb the octane, even after substantial time. The images from this experiment are shown in **Figure 12**.

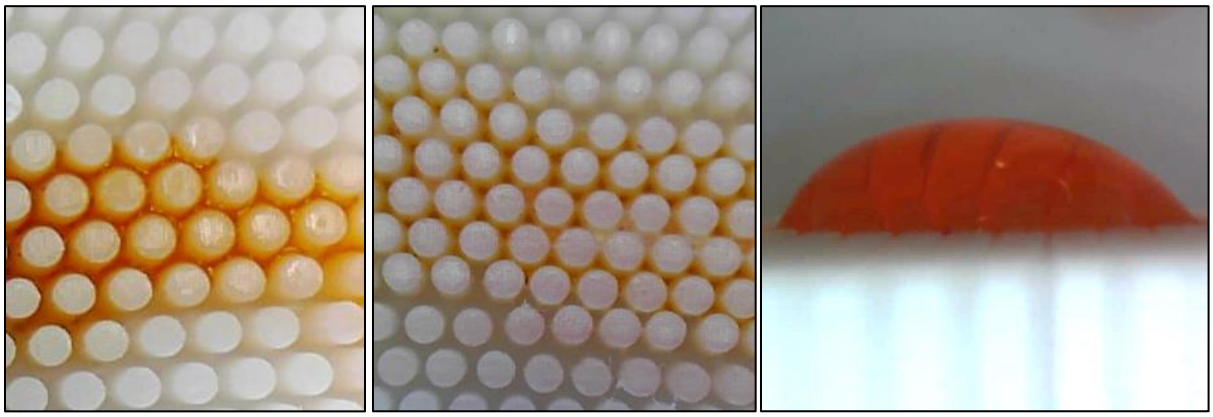

Figure 12: Images of a drop of octane, dyed with orange food coloring, on nonmodified (left), OTS modified (center), and FTS modified (right) new 3D printed models.

Using the same models as in the octane absorption experiment, the separation of a water and octane mixture was investigated. The results showed that the untreated model was able to absorb the octane rapidly, but also the displacement of the trapped air by the octane caused an increased absorption of the water in between the surface pillars. The OTS model only absorbed the octane and the water remained on top of the surface, unaffected by the air displacement caused by the octane. The FTS model absorbed neither the octane nor water, and instead the octane slightly spread out on top of the surface and the water drop remained in a semi-spherical shape on top of the octane. Images from this experiment are shown in **Figure 13** and additional images can be found in **Appendix D**.

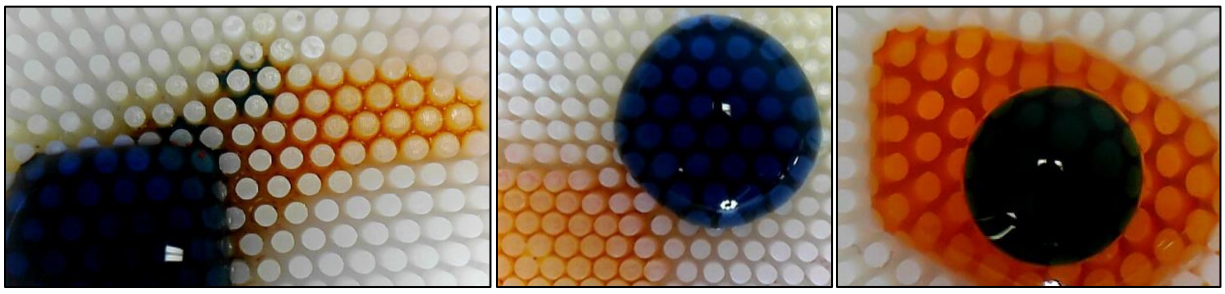

Figure 13: Images of a drop of octane, dyed with orange food coloring, and water, dyed with blue food coloring, on untreated (left), OTS modified (center), and FTS modified (right) new 3D printed models.

Lastly, for the uptake experiments, three models were printed in long strips with diameters of 0.5 mm, edge to edge spacing of 0.25 mm and heights of 1 mm. One model was oxidized, another was treated with OTS, and the final was treated with FTS. When using water, only the oxidized surface showed any uptake as well as retained water once removed from the reservoir. For octane, the oxidized surface showed the most amount of uptake, the OTS the second most and FTS none. In summary, the oxidized model absorbed octane the best, but it has a drawback of

also absorbing water, while the OTS model was effective at absorbing octane, and did not absorb any water. The heights traveled by each liquid on each model is shown in **Table 1** and images taken at the maximum uptake height are shown in **Figure 14**. The residual amount of liquid trapped between the pillars after removing the model from the reservoir is shown in **Figure 15**.

Table 1: A summary of the uptake heights for water and octane for each of the three models. The maximum height for each of the octane experiments occurred by 20 seconds and the water uptake of the oxidized surface by 10 seconds.

	Oxidized Surface		OTS Treated Surface		FTS Treated Surface	
	Water	Octane	Water	Octane	Water	Octane
Initial Height (mm)	0	13.7	0	9.9	0	0
Maximum Height (mm)	0.5	15.5	0	10	0	0

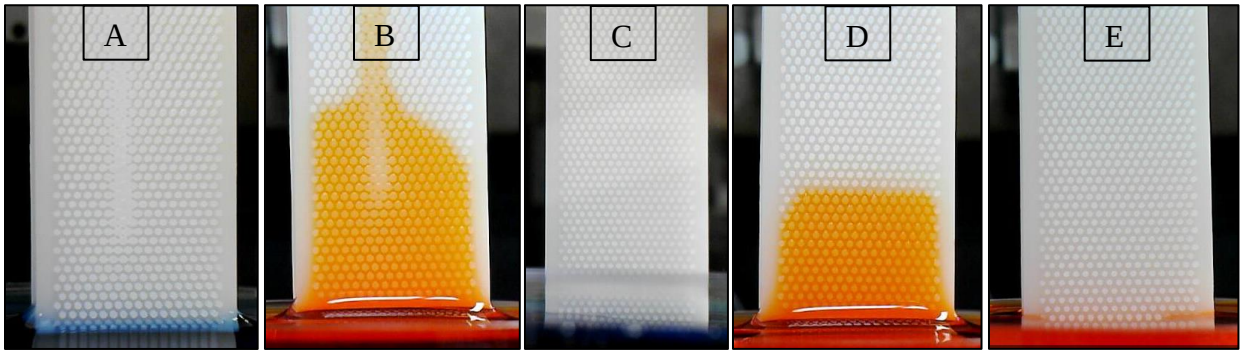

Figure 14: Images of the maximum uptake amount for water (blue) or octane (orange) on 3D printed models with varied surface treatments. A) Oxidized surface in water. B) Oxidized surface in octane. C) OTS surface in water. D) OTS surface in octane. E) FTS surface in octane. Not pictured is the FTS surface in water since there was not any uptake.

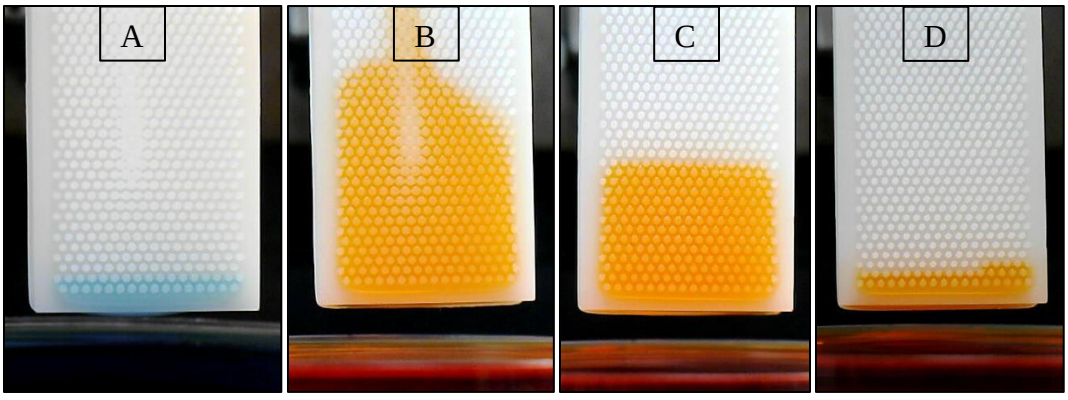

Figure 15: Images of the residual liquid trapped between the surface pillars for water (blue) or octane (orange) on 3D printed models with varied surface treatments. A) Oxidized surface in water. B) Oxidized surface in octane. C) OTS surface in octane. D) FTS surface in octane. Not pictured is the FTS or OTS surfaces in water since there was not any residual liquid left on the surface after removing it from the liquid.

Discussion and Analysis

This project aimed to expand on previous work to explore the idea of fabricating uniform textured surfaces that have hydrophobic properties, as done by plants and animals in nature. One example of a naturally occurring hydrophobic surface are cicada wings which feature a uniform array of microscopic pillars that trap air between them and thus repel water. Hydrophobic surfaces are useful for a variety of applications such as oil recovery, water purification, self-cleaning surfaces, anti-fouling, anti-fogging, and corrosion prevention.

The first goal of this project was to investigate ways to improve the quality of the 3D printed models. The previously fabricated models had problems with pillar uniformity and had dome shaped tops which resulted in contact angle hysteresis. A new printer and resin material, The Flashforge Foto 8.9 4K Mono LCD Resin 3D Printer with Anycubic 405 nm UV sensitive white resin, was selected to improve the quality of the models. This printer has a layer resolution of 25 mm and an accuracy of 50 mm and was determined to be one of the more affordable options with these specifications[6]. Additionally, the printing parameters and cleaning methods were adjusted through several trials to obtain the desired results.

The new 3D printed models were proven to be more accurate to the computer designed models and had less deviation in the measured pillar height and diameters compared to old models of the same design parameters. Also, the new models have flat tops instead of the dome shaped tops of the old models, this was proven to minimize the contact angle hysteresis since the contact area between the pillar tops and water drop was reduced. Overall, this means that the new printing capabilities produce models that are closer to the intended design. Additionally, when testing water droplet contact angles on the new and old models it was found that the new models perform just as well as the old ones and, in some cases, outperform the old models. This provides increased confidence in the new printing procedure as a viable method for fabricating models needed in further analysis of developing hydrophobic surfaces.

After the new models were proven to work just as well as the old models at repelling water, the secondary goal of investigating the contact angles and uptake of water and octane for the purpose of separating the components was conducted. The models were either left untreated, treated with OTS or treated with FTS. When a drop of octane was placed on the surface of the model it was found that both the untreated and OTS models absorbed the octane while the FTS model did not. This is consistent with the results found by Isabel Moryan using the old models with the same surface treatments[5]. Next the same three models had a drop of a water and octane mixture placed on the surface. The untreated model absorbed the octane and mostly repelled the water, but some water penetrated the pillars due to the air between the pillars already being displaced by the octane. The OTS model absorbed the octane and effectively repelled the water. The FTS model repelled both the octane and the water. This result indicates that both the untreated and OTS treated models can separate a mixed drop of octane and water, but the OTS treated model was more effective at this.

The results of the mixed drop of oil and octane were reinforced by liquid uptake experiments conducted for each of the three threated surfaces in either pure water or octane. This time the untreated surface was oxidized to remove any impact from residual octane, water, or other contamination. The oxidized surface was the only surface to uptake any water, even though it only traveled 0.5 mm from the liquid contact line. This surface also performed the best for

uptake of octane having an uptake height of 15.5 mm. The OTS treated model did not uptake any water and did uptake octane to a height of 10 mm. The FTS treated model did not uptake either the water or octane. These results indicate that although the oxidized surface had the highest octane uptake height, the OTS treated surface performed the best since it was capable of octane uptake and repelling water.

In conclusion, this project successfully fabricated new, more uniform 3D models that show properties of a hydrophobic surface that, with additional surface energy modification, could be effective at selectively absorption of octane over water. Although, there are still some sources of error that should be further investigated such as defects between some of the pillars and the possibility that the surface treatments were not fully grafted onto the model's entire surface. These sources of error should be investigated in future work along with the completion of more uptake experiments with increased pillar height and testing the limits of the printer by creating smaller features that more closely resemble the examples seen in nature like the cicada wing.

Literature Cited

[1] Hwang J, Jeong Y, Park JM, Lee KH, Hong JW, Choi J. Biomimetics: forecasting the future of science, engineering, and medicine. Int J Nanomedicine. 2015 Sep 8;10:5701-13. doi: 10.2147/IJN.S83642. PMID: 26388692; PMCID: PMC4572716.

[2] Nørgaard, T., Dacke, M. Fog-basking behaviour and water collection efficiency in Namib Desert Darkling beetles. Front Zool 7, 23 (2010). https://doi.org/10.1186/1742-9994-7-23

[3] Elbourne, A., Dupont, M. F., Collett, S., Truong, V. K., Xu, X. M., Vrancken, N., Baulin, V., Ivanova, E. P., & Crawford, R. J. (2019). Imaging the air-water interface: Characterising biomimetic and natural hydrophobic surfaces using in situ atomic force microscopy. Journal of Colloid and Interface Science, 536, 363–371. https://doi.org/10.1016/j.jcis.2018.10.059

[4] Pineault, Hannah, "Wetting Transition on 3D-printed Featured Surface" (2021). Williams Honors College, Honors Research Projects. 1274. https://ideaexchange.uakron.edu/honors_research_projects/1274

[5] Moryan, Isabelle, "Wetting Transition on 3D-Printed Surfaces" (2022). Williams Honors College, Honors Research Projects. 1487. https://ideaexchange.uakron.edu/honors_research_projects/1487

[6] Flashforge Foto 8.9 4K mono LCD resin 3D printer higher print speed. Flashforgeshop. (n.d.). Retrieved March 24, 2023, from https://www.flashforgeshop.com/product/flashforge-foto-89-lcd-3d-printer-higher-speed-for-garage-kit-use?cID=31&gclid=CjwKCAjwue6hBhBVEiwA9YTx8Pr9c3IkBuYqzKhYreN2SkEXl6OaLGtxzWtM-NU_8FmNnlqJjp-bdRoCID4QAvD_BwE

[7] Contact angle goniometry - tensiometry. Nanoscience Instruments. (2022, February 18). Retrieved March 25, 2023, from https://www.nanoscience.com/techniques/tensiometry/

Appendices

Appendix A

Additional Images for 3D Model Dimensions Comparison

Surface: H=1mm D=0.5mm S=0.25mm - New

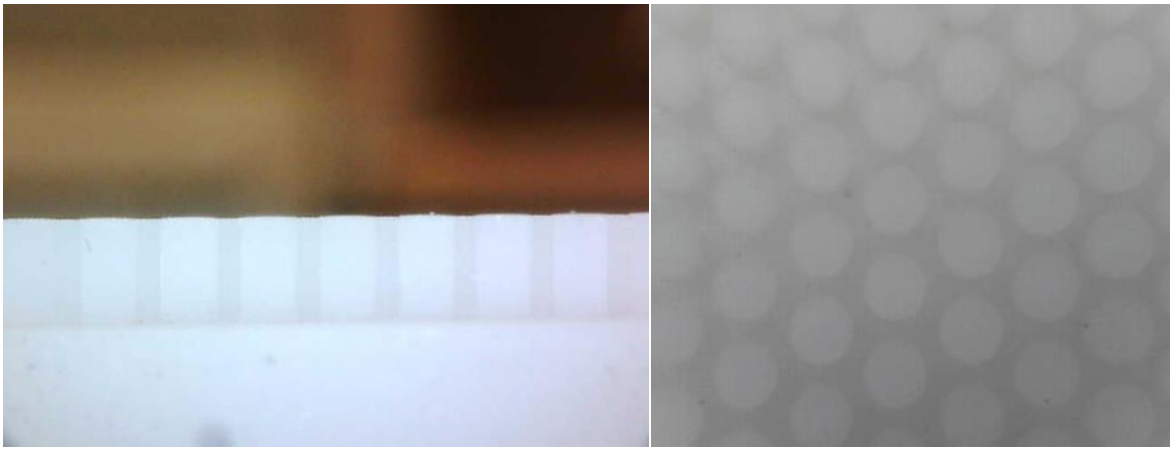

Surface: H=2mm D=0.5mm S=0.25mm - New

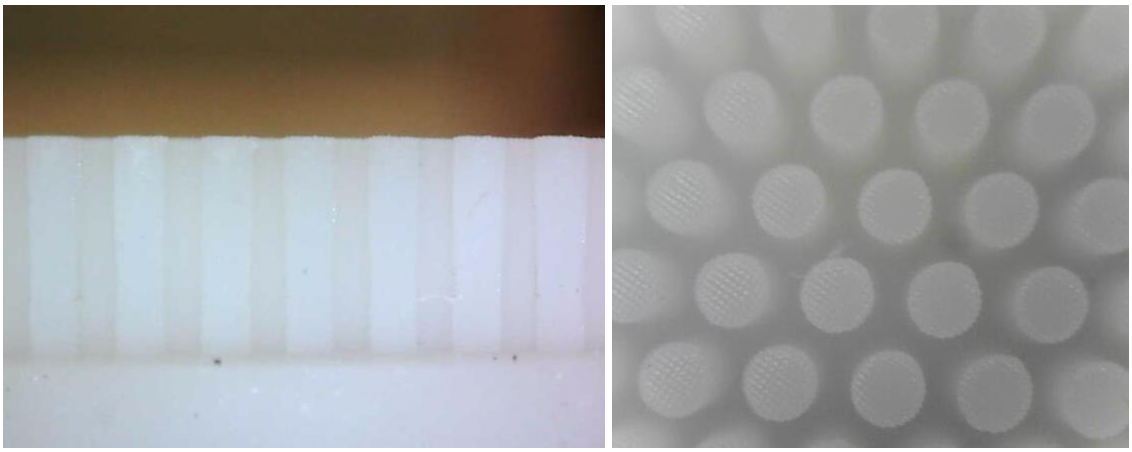

Surface: H=1mm D=0.5mm S=0.25mm – Old

Surface: H=2mm D=0.5mm S=0.25mm - Old

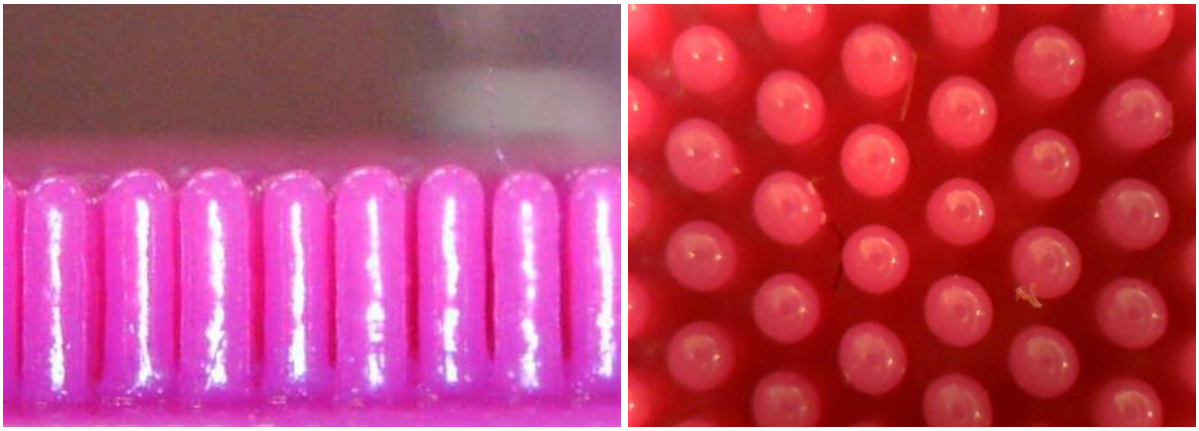

Appendix B

Measurements and Standard Deviations Comparing the New and Old Prints

Table B.1: Average heights and diameters for new and old 3D models along with respective standard deviation for each.

		Height (mm)		Diameter (mm)	
		Average	Standard Deviation	Average	Standard Deviation
H1 D0.5 S0.25	New	1.000	0.029	0.508	0.021
	Old	0.846	0.050	0.505	0.034
H1 D0.5 S0.25	New	1.992	0.022	0.496	0.015
	Old	1.820	0.103	0.494	0.024

T-Test Results for 3D Model Dimensions

	Old H1	*New H1*
Mean	0.846	1.000
Variance	0.003	0.001
Observations	15.000	15.000
Pooled Variance	0.002	
Hypothesized Mean Difference	0.000	
df	28.000	
t Stat	-10.294	
P(T<=t) one-tail	0.000	
t Critical one-tail	1.701	
P(T<=t) two-tail	0.000	
t Critical two-tail	2.048	

	Old D0.5 H1	*New D0.5 H1*
Mean	0.505	0.508
Variance	0.001	0.000
Observations	15.000	15.000
Pooled Variance	0.001	
Hypothesized Mean Difference	0.000	

df	28.000
t Stat	-0.289
P(T<=t) one-tail	0.387
t Critical one-tail	1.701
P(T<=t) two-tail	0.775
t Critical two-tail	2.048

	Old H2	*New H2*
Mean	1.820	1.992
Variance	0.011	0.000
Observations	15.000	15.000
Pooled Variance	0.006	
Hypothesized Mean Difference	0.000	
df	28.000	
t Stat	-6.322	
P(T<=t) one-tail	0.000	
t Critical one-tail	1.701	
P(T<=t) two-tail	0.000	
t Critical two-tail	2.048	

	Old D0.5 H2	*New D0.5 H2*
Mean	0.494066667	0.495533333
Variance	0.000577495	0.000218124
Observations	15	15
Pooled Variance	0.00039781	
Hypothesized Mean Difference	0	
df	28	
	-	
t Stat	0.201383769	
P(T<=t) one-tail	0.420927185	
t Critical one-tail	1.701130934	
P(T<=t) two-tail	0.841854371	
t Critical two-tail	2.048407142	

Appendix C

One-way ANOVA for Water Droplet Contact Angle Comparisons

Table C.1: Average water droplet contact angle on new and old 3D model surfaces when left untreated and when treated with OTS.

		Contact Angle on Untreated Surface		Contact Angle on OTS Treated Surface	
		Average	Standard Deviation	Average	Standard Deviation
H1 D0.5 S0.25	New	102.22	0.67	110.00	2.25
	Old	103.63	2.00	104.53	0.86
H1 D0.5 S0.25	New	101.43	1.57	107.99	6.81
	Old	107.80	4.88	103.71	2.75

Method

Null hypothesis	All means are equal
Alternative hypothesis	Not all means are equal
Significance level	α = 0.05

Equal variances were assumed for the analysis.

Analysis of Variance

Source	DF	Adj SS	Adj MS	F-Value	P-Value
Factor	7	339.0	48.42	4.20	0.002
Error	32	369.0	11.53		
Total	39	707.9			

Means

Factor	N	Mean	StDev	95% CI
New H1	5	102.216	0.674	(99.123, 105.309)
New H2	5	101.432	1.565	(98.339, 104.525)
Old H1	5	103.630	2.005	(100.537, 106.723)
Old H2	5	107.80	4.88	(104.70, 110.89)
OTS New H1	5	110.20	2.60	(107.11, 113.30)
OTS New H2	5	107.99	6.81	(104.90, 111.09)
OTS Old H1	5	104.526	0.862	(101.433, 107.620)
OTS Old H2	5	103.71	2.75	(100.62, 106.81)

Pooled StDev = 3.39558

Tukey Pairwise Comparisons

Grouping Information Using the Tukey Method and 95% Confidence

Factor	N	Mean	Grouping	
OTS New H1	5	110.20	A	
OTS New H2	5	107.99	A	B
Old H2	5	107.80	A	B
OTS Old H1	5	104.526	A	B
OTS Old H2	5	103.71	A	B
Old H1	5	103.630	A	B
New H1	5	102.216		B
New H2	5	101.432		B

Means that do not share a letter are significantly different.

Appendix D

Additional Images of Water/Oil Drop Separation

Untreated New Model Residual Water That Penetrated the Pillar Surface:

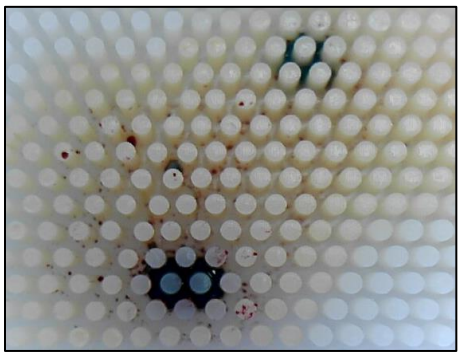

Untreated New Model Side View:

OTS Treated New Model Side View:

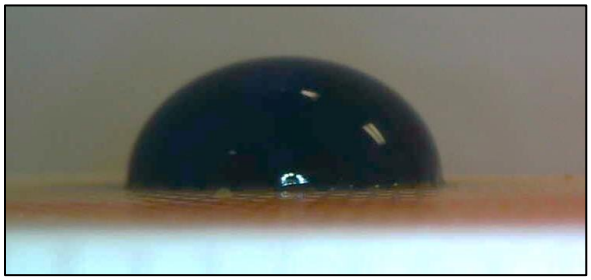

FTS Treated New Model Side View: